Analysis of Spatial Non-Stationary Characteristics for 6G XL-MIMO Communication

Weirang Zuo[1], Pan Tang[1], Haiyang Miao[1], Qi Wei[1], Lei Tian[1], Jianhua Zhang[1], Guangyi Liu[2], and Mengnan Jian[3,4]
[1]State Key Lab of Networking and Switching Technology,
Beijing University of Posts and Telecommunications, Beijing, China;
{zuoweirang; tangpan27; hymiao; weiqi0814; tianlbupt; jhzhang}@bupt.edu.cn.
[2]China Mobile Research Institute, Beijing, China;
liuguangyi@chinamobile.com.
[3]State Key Laboratory of Mobile Network and Mobile Multimedia Technology, Shenzhen 518055, China,
[4]Wireless Research Institute, ZTE Corporation, Beijing 100029, China;
jian.mengnan@zte.com.cn.

***Abstract*—Extremely Large-Scale Multiple-Input-Multiple-Output (XL-MIMO) communication, is recognized as a potential enabling technology for sixth-generation (6G) communication. Due to the large antenna aperture of XL-MIMO, spatial non-stationary (SnS) phenomena may occur on the array domain during deployment. This paper, relying on Ray-tracing (RT) simulations, analyzes the SnS phenomena from various perspectives of channel characteristics. Meanwhile, to accurately model the SnS phenomenon, this paper proposes a method for stationary sub-interval partitioning based on channel characteristics. It is assumed that the channel is stationary within each sub-interval, while it is non-stationary across different intervals. The method comprehensively considers factors such as channel correlation, delay spread (DS), azimuth angle spread of departure (ASD), and multipath components (MPCs) birth-death for sub-interval partitioning. By analyzing the independence of sub-intervals, this paper demonstrates that the proposed method performs better in sub-interval partitioning compared to the traditional averaging approach.**

***Index Terms*—6G, XL-MIMO, ELAA, spatial non-stationary, near-field, Ray-tracing.**

I. INTRODUCTION

With the fifth-generation (5G) wireless communication network entering the commercial deployment phase, the upcoming sixth-generation (6G) wireless communication network is gaining increasing attention [1] [2]. In December 2023, 2023 World Radiocommunication Conferences (WRC-23) [3] decided to explore the utilization of the mid-band for 6G communication in 2027. Currently, the 3rd Generation Partnership Project (3GPP) is intensively preparing the initiation of the second standard version, Rel-19, for 5G-Advanced. The emphasis is on enhancing and refining existing 3GPP channel models [4] by studying the near-field effects and SnS characteristics of channels in the mid-band 7-24 GHz.

When deploying Extremely Large-Scale Multiple-Input-Multiple-Output (XL-MIMO) [5] system with Extremely Large Antenna Arrays (ELAA), SnS phenomena may be observed on the array. The significant increase in antenna aperture in ELAA results in certain multipath signals being visible to only a subset of antennas while remaining invisible to others. This phenomenon is referred to as the SnS phenomenon [6]. In [7], outdoor measurements with a 256-element virtual uniform rectangular array (URA) were conducted at 6 GHz and 11 GHz. In [8], outdoor measurements with 40 × 40 virtual UPA antenna were conducted at the center frequency of 15 GHz. And analyzed the variations in the Rice K-factor, time delay spread, angle spread, and cluster characteristics within the array domain. In these measurement activities, the SnS phenomenon was observed consistently. The presence of SnS phenomena implies that the channels observed by different array elements are distinct. Characterizing the SnS phenomenon accurately in the model poses a challenge [9] [10]. Currently, some efforts characterize SnS phenomena by partitioning the array into different sub-intervals [11]. In [12], the channel data is processed in intervals of every 10 arrays, and the channel within each sub-interval is considered to be wide-sense stationary. In [8], the 1600-element array is split into multiple 7 × 7 sub-arrays, and SnS characteristics are analyzed based on these sub-arrays. In [13], SnS channel conditions are delineated by establishing a correspondence between sub-arrays and scatterers. The estimation of near-field SnS channels is then carried out from the viewpoint of sub-arrays. However, in these studies, the partitioning of sub-intervals is based on empirical averaging and does not take into account the impact of varying sub-interval sizes on channel analysis. There is currently a lack of systematic research on the stationary sub-interval partitioning method.

To fill the above gaps, a method for partitioning stationary sub-intervals based on channel characteristics is proposed and validated based on Ray-tracing (RT) simulations in this paper. The contributions of this paper are as follows:

- Based on Ray-tracing (RT) simulations, this paper analyzes SnS phenomena on a uniform linear array (ULA) in an indoor environment. By observing the variations of channel correlation, delay spread (DS), azimuth angle

979-8-3503-8741-4/24/$31.00 ©2024 IEEE

TABLE I
SIMULATION SETUPS

Parameter	Value
Frequency	13 GHz
Tx and RX height	1.8 m
Number of TX array elements	256
Number of RX array elements	1
Number of measuring points	6
Number of MPCs	25
Polarization	Vertical
Antenna type	Omnidirectional

spread of departure (ASD), and the birth-death of multi-path components (MPCs) on the array domain, it is found that these characteristics exhibit a partitioned distribution on the antenna array. The fluctuation of characteristic parameter values within the intervals is minimal, while significant changes are observed between different intervals, attributed to the variations in channel environments across distinct intervals.

- This paper proposes a method for stationary sub-interval partitioning by combining channel correlation, DS, ASD, and the MPCs birth-death. Utilizing RT simulation data, the proposed method is compared with the traditional averaging partitioning method. Through an analysis of sub-interval independence, the paper validates that the proposed method exhibits higher robustness and accuracy. It enables a more precise characterization of SnS phenomena.

The rest of this paper is organized as follows. Section II introduces the simulation scenario and parameter configurations. In Section III, We analyzed SnS phenomena from different perspectives of channel characteristics. Section IV provides a detailed description of the process for partitioning stationary intervals and validates the high accuracy and robustness of the proposed methods. Finally, Section V summarizes the entire document.

II. SIMULATION SETTINGS

Compared to the Sub-6 GHz or millimeter-wave frequency bands, there is a limited number of measurement samples within the 7-24 GHz mid-band. The industry lacks comprehensive channel characterization and performance comparisons for the channels within mid-band [14].

Against this background, this paper chooses to investigate the channel characteristics at a center frequency of 13 GHz. The simulation scenario is illustrated in Fig. 1, and the RT simulator is used to model this scenario. Tab. I lists the key configurations of the simulation. Utilizing a Uniform Linear Array (ULA) composed of omnidirectional antennas as the transmitting end (TX) and a single omnidirectional antenna as the receiving end (RX). The element spacing between adjacent antennas is set to $\lambda/2$, where λ represents the wavelength at 13 GHz. The channel parameters for RT simulation are generated using the commercial ray-tracing simulator Wireless Insite [15].

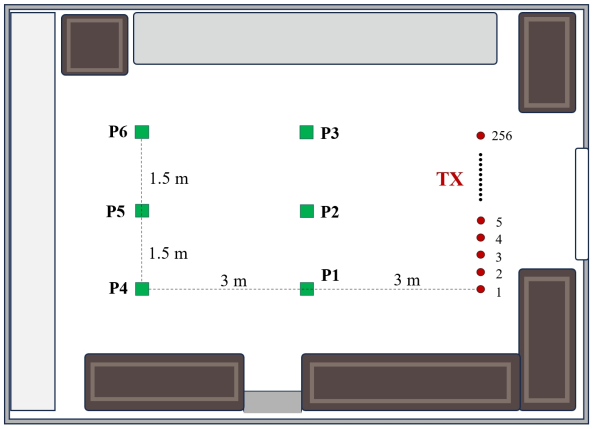

Fig. 1. The Ray-tracing Indoor simulation scenario.

III. ANALYSIS OF SPATIAL NON-STATIONARY PHENOMENA

In this section, We conducted an analysis of SnS phenomena from the perspectives of channel correlation, ASD, DS, and MPCs birth-death, respectively.

A. Analysis of Correlation

Based on simulation data, the channel impulse response (CIR) of arrays in this indoor scenario can be obtained. From this, the sub-CIRs for each transmitter array element can be extracted. Subsequently, the correlation between sub-channels can be assessed using the Frequency Response Assurance Criterion (FRAC) [16]

$$\rho_{ij} = \frac{\left|\sum_{n=1}^{N} h_i(\tau_n) h_j^*(\tau_n)\right|^2}{\sum_{n=1}^{N} h_i(\tau_n) h_i^*(\tau_n) \sum_{n=1}^{N} h_j(\tau_n) h_j^*(\tau_n)}, \tag{1}$$

where N and $(\cdot)^*$ are the number of delay bin and the Hermitian transpose, respectively, h_i and h_j represent the CIR of the i-th and j-th elements, respectively, ρ_{ij} represents the correlation between the channel of the i-th array element and the channel of the j-th array element, $\rho_{ij}^A \in [0,1]$ with $\rho_{ij}^A = 1$ indicating a perfect match of the i-th element CIR and the j-th element CIR.

The channel correlation matrix can be obtained by leveraging the correlation coefficients among all array elements. The resulting correlation matrix for the transmitter antenna is illustrated in Fig. 2. In this figure, both the horizontal and vertical axes represent the indices of the transmitter antenna elements. The values within the matrix denote the inter-channel correlation coefficients corresponding to the coordinates of the rows and columns. Larger values indicate a stronger correlation between elements. The correlation matrix displays a distinct block-like distribution, as evident in the figure. Within each block, the correlation coefficients display significant values with minimal fluctuations. This block-like pattern in the correlation matrix is ascribed to disparities in the scattering environment. Elements within the same interval block share similar scattering environments, resulting in

higher correlation coefficients. Conversely, differences in the scattering environment between distinct blocks lead to reduced correlation among elements. Hence, the correlation matrix displays a distinct block-like distribution. Also from the figure, it can be seen that the channel correlation between arrays decreases with increasing array spacing. This is because the difference in scattering environments between components that are farther apart is greater, resulting in a lower correlation.

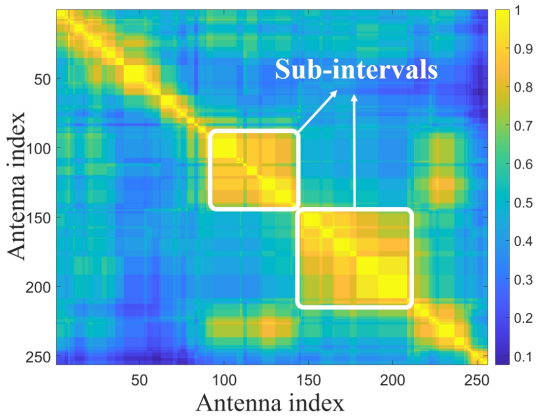

Fig. 2. Correlation matrix heatmap.

B. Analysis of DS and ASD

Multipath signals arrive at the receiver along different paths, causing the channel to exhibit both time-selective fading and space-selective fading. Among these, DS and ASD are crucial parameters of multipath signals, characterizing the distribution of multipath signals in the time and space domains, respectively.

As a vital parameter in multipath signals, DS can be extracted from the power delay profile. The statistical results of RMS DS serve as a primary indicator for assessing the time dispersion of wideband multipath channels. It effectively characterizes the abundance of MPCs within the channel. The RMS DS, denoted as τ_{rms}, is defined as the second-order central moment of the power delay profile and can be calculated using the following equation [17]

$$\tau_{rms} = \sqrt{\frac{\sum_{m=1}^{M}(\tau_m - \tau_{mean})^2 P(\tau_m)}{\sum_{m=1}^{M} P(\tau_m)}}, \tag{2}$$

where τ_m is the m-th delay bin, M is the number of delay bins, $P(\tau_m)$ is the corresponding delay bin power, τ_{mean} is the mean delay expressed as

$$\tau_{mean} = \frac{\sum_{m=1}^{M} \tau_m P(\tau_m)}{\sum_{m=1}^{M} P(\tau_m)}. \tag{3}$$

The computation of ASD closely resembles that of DS. It entails the power-weighted averaging of angles corresponding to different propagation paths of multipath signals. Utilize the method of cyclic angle extension as defined in 3GPP to mitigate the issue of angle ambiguity. [18].

At the same location, calculate DS and ASD values for all transmitting array elements, and analyze their variations on the array domain, as illustrated in Fig. 3. The horizontal axis represents the array index, while the vertical axis represents the values of DS and ASD. From Fig. 3, it can be observed that the variations of DS and ASD on the array domain are similar. This is because, with the evolution of the array domain, the scattering environment of antenna elements changes, leading to the occurrence of cluster birth-death on the array. The birth and death of these clusters simultaneously affect the temporal and spatial dispersion of MPCs signals. At the same time, the birth and death of clusters result in abrupt changes in the values of DS and ASD on the array domain. As parameter mutations are primarily induced by variations in the scattering environment, if the changes in DS and ASD within a sub-interval of the array are negligible, it can be inferred that all elements in this interval share the same scattering environment, and thus, there is no SnS phenomenon within this interval.

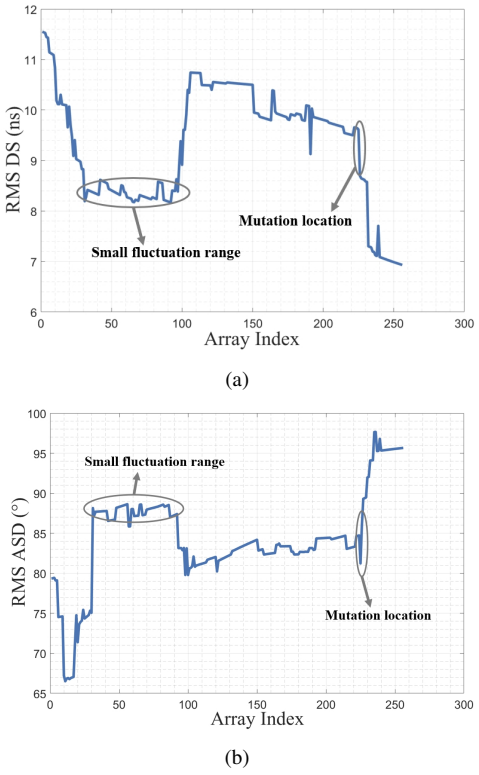

Fig. 3. (a) The changes of DS on the array domain. (b) The changes of ASD on the array domain.

C. Analysis of MPCs Birth-Death

The SnS phenomenon can also be reflected by the birth-death of MPCs. We therefore analyzed the variation of the angle of divergence (AOD) of MPCs over the array domain. The variation of AOD with the array is illustrated in Fig. 4, where the horizontal and vertical axes represent MPCs angles

and antenna index, respectively. The power difference of MPCs is reflected in the color changes.

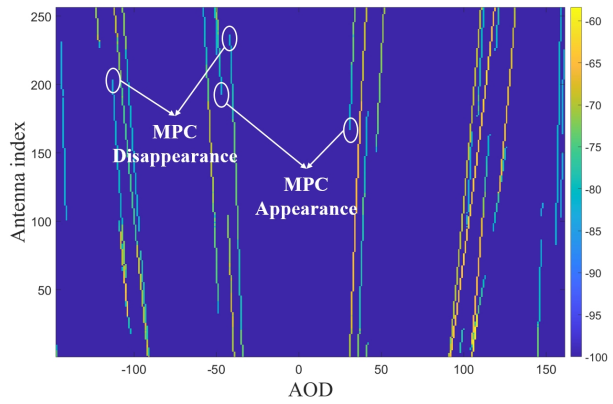

Fig. 4. The variation in the AOD of MPCs within the array domain reflects the birth and death of MPCs.

From Fig. 4, it can be observed that with the evolution of the array domain, the AOD of MPCs undergoes both continuous and discontinuous changes. The reason for the continuous variation is that when the distance between the transmitter and receiver is less than the Rayleigh distance [19], near-field effects exist, and the signal wavefront appears as a spherical wave. This results in continuous changes in the angles of MPCs on each antenna. On the other hand, the discontinuous variation is due to the large size of the array, which leads to differences in the scattering environments of different array elements, so that some MPCs may not be observed by all the antenna elements, resulting in the MPC birth-death phenomenon.

IV. Partition Method and Result Validation

A. Partition Method Process

This paper combines various channel characteristics, including MPCs birth-death, channel correlation, DS, and ASD, and proposes a method for array field stationary interval partitioning. The specific partitioning process is outlined as follows.

Firstly, based on RT simulation, we can obtain MPCs parameters data X, $X = \{x_1, x_2, \ldots, x_K\}$, where x_1 representing the MPCs parameters of the first array element, including power, delay, phase, and angles. Then we can calculate the CIR for each transmitting element, which is utilized for subsequent characteristic analysis.

After processing the parameters, we can proceed with the partitioning of stationary intervals based on the characteristic analysis in Section III. Initially, we preselect interval nodes based on MPCs birth-death, with the selection method outlined by the following expression

$$S(k) = \begin{cases} 1 & \text{if } p_k^n - p_{k-1}^n \geq 3\,\text{dB} \\ -1 & \text{if } p_k^n - p_{k-1}^n \leq -3\,\text{dB} \\ 0 & \text{else} \end{cases}, \tag{4}$$

where k belongs to the range 1 to K, K is the number of transmitting array elements, n belongs to the range 1 to N, N is the total number of MPCs from the k-th array element. The value of $S(k)$ represents the birth and death situation at the k-th element, $S(k) = 1$ indicates the birth of a new MPC at the k-th element, $S(k) = -1$ indicates the death of a MPC at this location, and $S(k) = 0$ indicates no birth or death phenomenon at the k-th element. The specific selection criterion is based on the power variation of multipath signals on the array domain. p_k^n represents the power of the n-th path at the k-th array element, and p_{k-1}^n represents the power of the n path at the $(k-1)$-th array element. If there exists a path for which $p_k^n - p_{k-1}^n \geq 3$ dB, then set $S(k) = 1$, when $p_k^n - p_{k-1}^n \leq 3$ dB, set $S(k) = -1$. By iterating through all elements, we obtain the complete S vector.

After obtaining the S vector, we still need to use channel correlation, DS, and ASD to further refine the selection of interval nodes. By analyzing the variations in parameters at the array element, select elements from S that can serve as interval boundaries. First, by analyzing changes in correlation, if a certain interval can be considered stationary, the correlation coefficients for sub-channels within that interval are relatively large and exhibit minimal fluctuations. When adding a new element to this interval, if the fluctuations significantly increase, the added element might be a boundary element. The fluctuation is calculated using the Mean Absolute Deviation (MAD).

$$MAD = \frac{1}{n}\sum_{i=1}^{n} |x_i - \bar{x}|, \tag{5}$$

where n is the number of the data, x_i represents the i-th data, and $\bar{x}$ is the mean of all data. For DS and ASD, a similar approach can be applied. If adding an element to an interval results in a substantial increase in parameter fluctuations, then this element might also be a boundary element. Jointly considering channel correlation, DS, and ASD, the following equation is used for assessment.

$$w_c \cdot \frac{M_k^C}{M_{k-1}^C} + w_a \cdot \frac{M_k^A}{M_{k-1}^A} + w_d \cdot \frac{M_k^D}{M_{k-1}^D} > \rho, \tag{6}$$

where M_k^C represents the fluctuation of channel correlation within the interval when the k-th element is chosen as the boundary, and M_{k-1}^C represents the fluctuation when the $(k-1)$-th element is taken as the boundary. Similarly, M_k^A and M_k^D measure the fluctuation of ASD and DS, respectively. w_c, w_a and w_d represent the weights assigned to the fluctuation values of correlation coefficient, ASD, and DS, respectively. ρ is the threshold for judgment. The inequality (6) is used to evaluate each element in S, and if the calculated result at a certain element exceeds the threshold, that element is considered a boundary node. After completing the traversal, the final interval partitioning result Z is obtained. Optimize the objective function to obtain the optimal weights and thresh-

olds, where $w_c = 0.45$, $w_a = 0.3$, $w_d = 0.25$, and $\rho = 0.006$. The objective function is defined as

$$D = \frac{1}{N \cdot (M-1)} \sum_{k=1}^{M-1} \sum_{i=1}^{N} |h_{k+1}(i) - h_k(i)|, \tag{7}$$

where N and M respectively represent the number of delay bins and sub-intervals, h_k represents the reconstruction CIR of the k-th sub-interval. We constructed delay bins by using timing information from all MPCs. Subsequently, we reconstructed CIR in different intervals using power and phase information. If there are multiple MPCs within a delay bin, average the power of these MPCs. The flow of the algorithm is shown in Algorithm 1.

Algorithm 1: Partition based on channel characteristics

```
Input X = {x_1, x_2, ..., x_K};
for i = 1 to K do
    Generate the CIR of the i-th array element;
for i = 1 to K − 1 do
    Generate pre-selected partition nodes S(i);
    for n = 1 to N do
        if p^n_{i+1} − p^n_i ≥ 3 dB then
            S(i) = 1;
            break;
        else if p^n_{i+1} − p^n_i ≤ −3 dB then
            S(i) = −1;
            break;
        else
            S(i) = 0;
Calculate channel correlation matrix, DS, and ASD;
for i = 1 to K do
    Generate the final partition node;
    if S(i) ≠ 0 && Satisfy inequality (6) then
        Z ← Z ∪ {i};
Output Z;
```

B. Result Analysis

The partitioning results are shown in the following Fig. 5. We demonstrate the partition results by depicting the distribution of ASD and DS in each sub-interval. Because average partitioning does not take into account the changes in channel characteristics, it may introduce two issues during the partitioning process. Firstly, average partitioning may classify array elements with similar scattering environments into two different sub-intervals. Secondly, it may group array elements with changing scattering environments into the same sub-interval. By using the method proposed in this paper, both of these issues can be avoided.

After completing the partitioning, we can obtain the reconstructed CIR for each sub-interval. Then using equation (7), we analyzed the independence of sub-intervals obtained based on channel characteristics and average partitioning, the results are shown in Fig. 6.

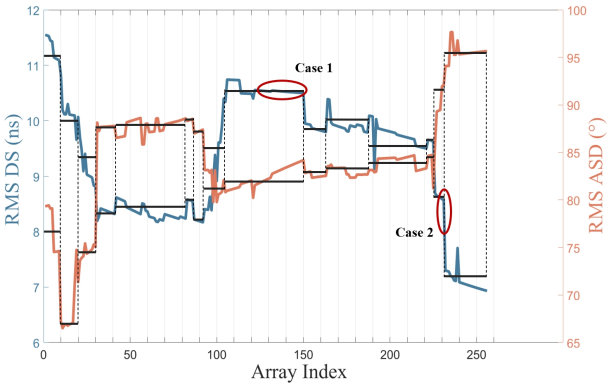

Fig. 5. Partition results diagram. Where the solid black line represents the partitioning results obtained in this paper, and the grid lines represent the results of averaging partitions with sub-intervals of 10.

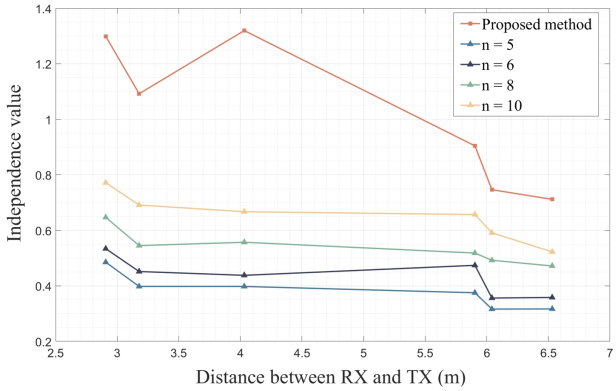

Fig. 6. The degree of independence of sub-intervals obtained by different partitioning methods. The n represents the number of array elements in each sub-interval during average partitioning.

In Fig. 6, the horizontal and vertical axes represent the TX-RX distance and independence level, respectively. It can be observed that, as traditional partitioning methods do not consider environmental factors, the independence of sub-intervals is influenced by the size of intervals, resulting in poor robustness. Conversely, when partitioning is based on channel characteristics, the method accurately assigns elements with different scattering environments to distinct intervals. As a result, the obtained results have higher accuracy and robustness. Additionally, it is observed that as the distance between the transmitter and receiver increases, the independence of sub-intervals decreases for different methods. This is because, with the increasing distance between the transmitter and receiver, SnS phenomena become less pronounced. When the distance exceeds the Rayleigh distance, the scattering environments in different sub-intervals become identical, and the independence of sub-intervals becomes zero.

V. CONCLUSION

This paper analyzes the SnS phenomena on the array domain from various channel characteristic perspectives. Based on the analysis results, a stationary sub-interval partitioning method is proposed. This method integrates various channel characteristics, including channel correlation, DS, ASD, and MPCs birth-death. A comparative analysis with traditional average partitioning is performed to validate that the proposed method achieves accurate partitioning results. For future work, to achieve stationary modeling in different intervals, the paper plans to conduct near-field channel measurements with large-aperture arrays in various scenarios. This aims to statistically analyze the distribution of sub-interval sizes and sub-interval parameters in different scenarios.

ACKNOWLEDGMENT

This research is supported in part by the National Natural Science Foundation of China (62201086, 62101069, 92167202), the National Science Fund for Distinguished Young Scholars (61925102), the Beijing University of Posts and Telecommunications-China Mobile Research Institute Joint Innovation Center, and the ZTE Industry-University-Institute Cooperation Funds.

REFERENCES

[1] J. Zhang, J. Lin, P. Tang et al., "Channel measurement, modeling, and simulation for 6G: A survey and tutorial." *arXiv preprint arXiv: 2305.16616.*, May. 2023.

[2] J. Zhang, P. Tang, L. Yu et al., "Channel measurements and models for 6G: current status and future outlook." *Frontiers of information technology & electronic engineering.*, vol. 21, no. 1, pp. 39-61, Jan. 2020.

[3] ITU, "World Radiocommunication Conference 2023 (WRC-23)." Available: https://www.itu.int/dms_pub/itu-r/opb/act/R-ACT-WRC.15-2023-PDF-E.pdf, Dec. 2023.

[4] 3GPP, "Study on channel model for frequencies from 0.5 to 100 GHz (Release 15)." *3GPP TR 38.901, Technical Report.*, Dec. 2017.

[5] E. Björnson, L. Sanguinetti, H. Wymeersch et al., "Massive MIMO is a reality-What is next?: Five promising research directions for antenna arrays." *Digital Signal Processing.*, vol. 94, pp. 3-20, Nov. 2019.

[6] Z. Yuan, J. Zhang, Y. Ji et al., "Spatial non-stationary near-field channel modeling and validation for massive MIMO systems." *IEEE Transactions on Antennas and Propagation.*, vol. 71, no. 1, pp. 921-933, Jan. 2023.

[7] J. Li, B. Ai, R. He et al., "Channel characterization for massive MIMO in subway station environment at 6 GHz and 11 GHz." in *IEEE Vehicular Technology Conference (VTC-Fall).*, pp. 1-5, Aug. 2018.

[8] J. Chen, X. Yin, X. Cai et al., "Measurement-based massive MIMO channel modeling for outdoor LoS and NLoS environments." *IEEE Access.*, vol. 5, pp. 2126-2140, Jan. 2017.

[9] J. Zhang, "Review of wideband MIMO channel measurement and modeling for IMT-Advanced systems." *Chinese science bulletin.*, vol. 57, no. 19, pp. 2387-2400, 2012.

[10] P. Zhang, J. Chen, X. Yang et al., "Recent research on massive MIMO propagation channels: A Survey." *IEEE Communications Magazine.*, vol. 56, no. 12, pp. 22-29, Dec. 2018.

[11] À. O. Martínez, P. Eggers and E. De Carvalho, "Geometry-based stochastic channel models for 5G: Extending key features for massive MIMO." in *IEEE International Symposium on Personal, Indoor, and Mobile Radio Communications (PIMRC).*, pp. 1-6, Sep. 2016.

[12] X. Gao, F. Tufvesson and O. Edfors, "Massive MIMO channels—measurements and models." in *2013 Asilomar Conference on Signals, Systems and Computers.*, pp. 280-284, Nov. 2013.

[13] Y. Han, S. Jin, C. Wen et al., "Channel estimation for extremely large-scale massive MIMO systems." *IEEE Wireless Communications Letters.*, vol. 9, no. 5, pp. 633-637, May. 2020.

[14] H. Miao, J. Zhang, P. Tang et al., "Sub-6 GHz to mmWave for 5G-Advanced and Beyond: channel measurements, characteristics and impact on system performance." *IEEE Journal on Selected Areas in Communications.*, vol. 41, no. 6, pp. 1945-1960, May. 2023.

[15] Remcom, "Wireless insite." [Online]. Available: https://www.remcom.com/wireless-insite.

[16] W. Heylen and S. Lammens, "FRAC: A consistent way of comparing frequency response functions." in *Proceedings of the conference on identification in engineering systems.*, pp. 48–57, Mar. 1996.

[17] H. Miao, P. Tang, J. Zhang et al., "Measurement-based massive MIMO channel characterization in 6 GHz band for 6G." in *IEEE Wireless Communications and Networking Conference (WCNC).*, Apr. 2024. (accepted).

[18] 3GPP, "Study on 3D channel model for LTE (Release 12)." *3GPP TR 36.873, Technical Report.*, 2014.

[19] K. T. Selvan and R. Janaswamy, "Fraunhofer and Fresnel Distances: Unified derivation for aperture antennas." *IEEE Antennas and Propagation Magazine.*, vol. 59, no. 4, pp. 12-15, Aug. 2017.

[20] N. Czink, P. Cera, J. Salo et al., "A framework for automatic clustering of parametric MIMO channel data including path powers." in *IEEE Vehicular Technology Conference.*, pp. 1-5, Sep. 2006.